2 mcy

X-671-73-370

PREPRINT

NASA TM X-70536

STUDIES OF HYDRODYNAMIC EVENTS IN STELLAR EVOLUTION. III. EJECTION OF PLANETARY NEBULAE

WARREN M. SPARKS

G. S. KUTTER

DECEMBER 1973

GSFC — GODDARD SPACE FLIGHT CENTER —

GREENBELT, MARYLAND

Studies of Hydrodynamic Events in Stellar Evolution. III.

Ejection of Planetary Nebulae

G. S. KUTTER

The Evergreen State College, Olympia, Washington

WARREN M. SPARKS

NASA-Goddard Space Flight Center, Greenbelt, Maryland

Received _____

Abstract

We investigate the dynamic behavior of the H-rich envelope (0.101 $M_\odot$) of an evolved star (1.1 $M_\odot$) as the luminosity rises to 19000 $L_\odot$ during the second ascent of the red giant branch.

For luminosities in the range $3100 < L < 19000\ L_\odot$ the H-rich envelope pulsates like a long-period variable (LPV) with periods of the order of a year. As L reaches 19000 $L_\odot$, the entire H-rich envelope is ejected as a shell with speeds of a few 10 km s^{-1}. The ejection occurs on a timescale of a few LPV pulsation periods. We connect this ejection with the formation of a planetary nebula.

Our computations are based on an implicit hydrodynamic computer code. T- and ρ -dependent opacities and excitation and ionization energies are included. As the H-rich envelope is accelerated off the stellar core, we approximate the gap between envelope and core by a vacuum, filled with radiation. Across the vacuum we conserve the luminosity and we take into account the anisotropy of the radiation as well as the solid angle subtended by the remnant star at the inner surface of the H-rich envelope. We assume spherical symmetry and the diffusion approximation.

I. Introduction

We are continuing our theoretical investigation of ejection of planetary nebulae. In Studies of Hydrodynamic Events in Stellar Evolution. II (Sparks and Kutter 1972, hereafter referred to as Paper II) we showed that the H-rich envelopes of red giants become dynamically unstable when the luminosity exceeds a limiting value L_o. For a constant opacity, $L_o \simeq 10^{3.3}((M/M_\odot)/\kappa)L_\odot$. When $L > L_o$, the envelope expands as a shell with final velocities of a few km s^{-1} and rates of mass flow of 10^{-5} to $10^{-4} M_\odot$ yr^{-1}. This mass ejection is driven by transfer of momentum and energy from the radiation to the gas. We suggested that, depending on the structure of the envelope and the value of the luminosity, these instabilities may be responsible for the pulsation of long-period variables, the ejection of planetary nebulae, and the formation of some infrared objects. Further, planetary nebula ejection seems to be always preceeded by long-period variability (Sparks and Kutter 1971).

This mechanism for long-period variables was first proposed by Paczyński and Ziołkowski (1968 a,b) and thoroughly explored by Keeley (1970) and by Wood (1973). The connection with planetary nebulae ejection dates back to Jeans (1923). Kutter, Savedoff, and Schuerman (1969) revived this possibility and included the contribution of gas pressure in their analytical treatment. In Paper II we continued this work, using an implicit hydrodynamic computer code (Kutter and Sparks 1972, hereafter called Paper I). We assumed (1) spherical symmetry, (2) diffusion approximation, (3) constant opacity, and (4) complete ionization.

In order to investigate the dynamic behavior of red giant envelopes under

more realistic conditions, we next included T- and ρ-dependent opacities and ionization and excitation energies (Sparks and Kutter 1973). We found that the ejection of the H-rich envelope is qualitatively the same as in Paper II. However, there exists no simple formula for L_o. For a 1.1 $M_\odot$ star, the envelope is ejected for luminosities exceeding $1.4 \cdot 10^4$ $L_\odot$.

In none of our investigations up to this point did we allow the H-rich envelope to actually separate from the stellar core. Thus, as the H-rich envelope expands, its innermost Lagrangian zone and the outermost Lagrangian zone of the stellar core are stretched out to widths comparable to their radii. Under these circumstances, both the mathematical (replacement of differentials by differences) and the physical descriptions become invalid. In the present investigation we correct for these defects by introducing a vacuum, filled with radiation, between the stellar core and the H-rich envelope whenever the inner surface of the H-rich envelope is accelerated faster than the outer surface of the core. Across the vacuum we conserve the luminosity (instead of the radiation flux) and we take into account the anisotropy of the radiation as well as the solid angle subtended by the remnant star at the inner surface of the H-rich envelope. We still keep assumptions (1) and (2) above.

As in Paper II, we raise the luminosity of our stellar model to the range observed for planetary nuclei. In one of the evolutionary runs we include the opacity of water vapor, which sets a lower limit between 10^{-4} to 10^{-3} $cm^2 g^{-1}$ and, thus, raises the optical thickness of the H-rich envelope when its temperature drops below about 2500 ^oK.

II. Mathematical Formulation

Our stellar model is taken from Paper II. It is a red giant of 1.1 $M_\odot$ with a He shell of 0.075 $M_\odot$ and a H-rich envelope of 0.101 $M_\odot$ surrounding a

core. The core is replaced by boundary conditions specifying r, u, and L.

The He shell is assumed to be completely ionized, with $\kappa = 0.19\ cm^2\ g^{-1}$ (electron scattering). The H-rich envelope consists of the Aller mix (X = 0.596, Y = 0.384, Aller 1961). Tables of opacity, internal energy, and excitation, ionization and molecular binding energies come from A. Cox and his collaborators at the Los Alamos Scientific Laboratory. Their opacity tables do not include the contribution of H_2O, although below 2500 °K water becomes the dominant opacity source (Auman 1966). We take the H_2O opacity from Auman and Bodenheimer (1967), but we neglect the H_2O binding energy.

We begin our model computations with the age zero model of Paper II. In steps we increase the luminosity at the base of the He shell to $1.9 \cdot 10^4\ L_\odot$. The radius at this base is kept at $2 \cdot 10^9$ cm. This simulates the evolution of the outer part of the star during its second ascent up the red giant branch. The high luminosity originates in the He shell, due either to quiescent nuclear burning (Kutter 1971) or to a thermal runaway (Rose and Smith 1970), as well as by gravitational contraction of the core.

To save computer time, we use the two-timing method in the He shell: the term $\partial L/\partial m$ in the equation of conservation of energy is multiplied by 1000 (Talbot 1971a, b). This increases the radiative diffusion timescale through the He shell to roughly the evolution timescale of the H-rich envelope. After every time step we compute the acceleration at the outer surface of the He shell, $\ddot{r}_a$ (see Section III), and at the inner surface of the H-rich envelope, $\ddot{r}_b$. When $\ddot{r}_a < \ddot{r}_b$, the H-rich envelope separates from the He shell and we introduce the vacuum.

Unless otherwise specified, the computing method and the notation are those used in Paper II and described in Paper I. At any given time step, we iterate until the results $\left\{ u_i,\ B_i,\ R_i,\ W_{i+1/2},\ Z_{i+1/2} \right\}$ satisfy the 5

difference equations (Paper I, equ. 8 - 12) to within 0.01 % for all Lagrangian zones. The parameter θ (Paper I) is set equal to 1. In convective zones we set the mixing length equal to the pressure scale height. The stellar model is divided into 100 Lagrangian zones, with the first 17 belonging to the He shell.

III. The Vacuum

The code described in Paper I has, per Lagrangian zone, 5 first-order differential equations and 5 dependent variables, u_i, L_i, r_i, $\rho_{i+1/2}$, $T_{i+1/2}$. Introducing the vacuum requires 7 first-order differential equations and 7 dependent variables. Let j refer to the composition discontinuity. Upon separation let a refer to the outer surface of the He shell and b to the inner surface of the H-rich envelope:

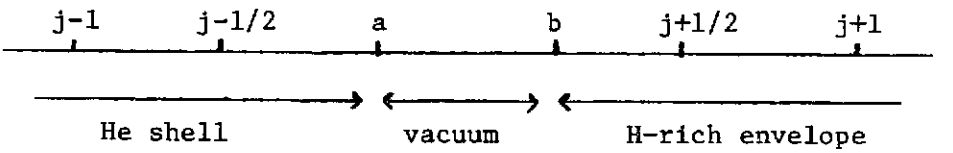

The 7 dependent variables are u_a, u_b, $L_a = L_b$, r_a, r_b, $\rho_{j+1/2}$, $T_{j+1/2}$. The 7 differential equations are those described in Paper I except (1) there are two difference equations for momentum conservation, one between j-1/2 and a, the other between b and j+1/2; (2) the velocity is defined at points a and b; and (3) the radiative luminosity becomes a function of $r_{j-1/2}$, r_a, r_b, $r_{j+1/2}$, $\rho_{j-1/2}$, $\rho_{j+1/2}$, $T_{j-1/2}$, $T_{j+1/2}$.

The expression for L is derived from the radiative transfer equation

$$\frac{1}{c}\frac{dI}{dt} \equiv \frac{1}{c}\frac{\partial I}{\partial t} + \hat{s}\cdot\nabla I = -\kappa\rho(I - S), \qquad (1)$$

where in general the intensity, I, and source function, S, are functions of

position, direction ($\hat{s}$), and time. In the present work we neglect the term $\frac{1}{c}\frac{\partial I}{\partial t}$ because of the relatively slow variation of the radiation flow. We assume spherical symmetry, a gray atmosphere, and isotropy for S. Across the vacuum, we conserve the luminosity and we assume that the radiation has two components, I_a and I_b, which are emitted isotropically at a and b, respectively. With these simplifications, equation (1) reduces to the familiar form

$$\cos\theta \frac{\partial I}{\partial \tau} = I - S, \tag{2}$$

where the optical thickness, τ, is measured either from r_a toward $r_{j-1/2}$ or from r_b toward $r_{j+1/2}$.

At point a the radiative energy density, flux, and pressure are

$$E_a = \frac{2\pi}{c}\left(I_a + I_b\right), \quad \text{erg cm}^{-3}, \tag{3a}$$

$$\mathcal{F}_a = \pi\left(I_a - I_b\right), \quad \text{erg cm}^{-2}\ \text{s}^{-1}, \tag{3b}$$

$$P_a = \frac{2\pi}{3c}\left(I_a + I_b\right), \quad \text{dyne cm}^{-2}. \tag{3c}$$

At point b, they are

$$E_b = \frac{2\pi}{c}\left[I_a\left(1 - X_b\right) + I_b\left(1 + X_b\right)\right], \quad \text{erg cm}^{-3}, \tag{4a}$$

$$\mathcal{F}_b = \pi\left(I_a - I_b\right)\left(1 - X_b^2\right), \quad \text{erg cm}^{-2}\ \text{s}^{-1}, \tag{4b}$$

$$P_b = \frac{2\pi}{3c}\left[I_a\left(1 - X_b^3\right) + I_b\left(1 + X_b^3\right)\right], \quad \text{dyne cm}^{-2}; \tag{4c}$$

where $X_b = (1 - r_a^2/r_b^2)^{1/2}$. In this section, all pressures with subscripts j+ 1/2 refer to the sum of gas and radiation pressures; the others (P, P_a, P_b) refer to radiation pressure only.

From equation (3b) we derive

$$L_a = 4\pi^2 r_a^2 \left(I_a - I_b\right). \tag{5}$$

Applying the diffusion approximation between points j-1/2 and a, the definition $I_a \equiv \frac{\sigma}{\pi} T_a^4$, and replacing differentials by differences, we obtain

$$I_a = \frac{\sigma}{\pi}\left[\overline{T}^4_{j-\frac{1}{2}} - \frac{3 L_a}{16\pi\sigma r_a^2}\left(\tau_{j-\frac{1}{2}} - \frac{2}{3}\right)\right]. \tag{6}$$

Next we need an expression for L between points b and j+1/2. From equation (2) we derive

$$4\pi r^2 c \frac{\partial P}{\partial \tau} = - L. \tag{7}$$

Integrating by parts and assuming that P and r are related via the expression $\partial \ln P / \partial \ln r = -n$, we obtain

$$L_b = \frac{4\pi c}{\tau_{j+\frac{1}{2}}} \frac{n}{n-2}\left(r_b^2 P_b - r^2_{j+\frac{1}{2}} P_{j+\frac{1}{2}}\right). \tag{8}$$

Substituting in equation (8) for P_b (equation [4c]) and then for I_a (equation [4b]) leads to

$$L_b = \frac{16\pi\sigma r_b^2}{3} \frac{\frac{\pi}{\sigma} I_b - \frac{r^2_{j+\frac{1}{2}}}{r_b^2}\overline{T}^4_{j+\frac{1}{2}}}{\frac{n-2}{n}\tau_{j+\frac{1}{2}} - \frac{2}{3}\frac{1-X_b^3}{1-X_b^2}}. \tag{9}$$

The number n cannot be determined as part of the solution; it is taken from the previous time step. If $L > 0$, then $n > 2$. For $\gamma = 4/3$, $n = 4$; while in the plane parallel case $n \longrightarrow \infty$.

Finally from equations (5), (6), and (9) we derive our desired expression for the luminosity,

$$L_a \equiv L_b = \frac{16\pi\sigma}{3} r_a^2 \frac{\overline{T}^4_{j-\frac{1}{2}} - \frac{r^2_{j+\frac{1}{2}}}{r_b^2}\overline{T}^4_{j+\frac{1}{2}}}{\frac{n-2}{n}\left(1-X_b^2\right)\tau_{j+\frac{1}{2}} + \tau_{j-\frac{1}{2}} + \frac{2}{3}X_b^3}. \tag{10}$$

In the present investigation, j = 18. The numerical solution of these 7 difference equations proceeds via the linearization and Gaussian elimination scheme presented in Paper I.

IV. Results

In Section IV.a we summarize the evolution of the stellar model as L $\longrightarrow$ 19000 $L_\odot$. We then describe in detail the ejection of the envelope for the run including H_2O opacity. In Section IV.c we summarize the run without H_2O opacity.

a. Evolution to 19000 $L_\odot$

As we raise the luminosity at the base of the He shell, the H-rich envelope pulsates like a long-period variable (LPV). The pulsations are driven by the exchange of momentum and energy between radiation and gas in the optically thick part of the envelope, due to the γ- and κ-mechanisms (Keeley 1970, Paper II, Sparks and Kutter 1973). In table 1 we summarize the physical conditions at optical depth 1 ($\bar{\tau} = 1$) for several values of L. These results are consistent with the observational data of LPV's (Allen 1963).

Beyond 8000 $L_\odot$, the H-rich envelope becomes progressively more extended with a sharp discontinuity in the values of the physical parameters at the composition interface. At 19000 $L_\odot$, the H-rich envelope separates from the He shell according to the condition given in Section III. From here on we hold the luminosity at the base of the He shell constant, delete the two-timing method, set the age Λ equal to zero, and include the vacuum routine in our computations.

b. Ejection of H-rich envelope, H_2O opacity

In table 2 we summarize the physical conditions of the H-rich envelope at age zero. The outward acceleration now begins to dominate the pulsation. Within a few years the velocity of the entire envelope exceeds escape velocity, its inner radius surpasses 10 A.U., and eventually it becomes optically thin in the continuum.

The main features of the ejection of the H-rich envelope, including H_2O, are the following.

1. At age zero the H-rich envelope is optically thin to Q = 0.0235 (Q = 1 - m/M_o, fractional stellar mass exterior to m). During the initial phase of ejection the point $\bar{\tau} = 1$ fluctuates back and forth somewhat in Lagrangian coordinates, although on the average it moves inward. The fluctuation is caused (1) by very weak, remnant envelope pulsations, which are superimposed on the expansion; (2) by moderate numerical shocks (artificial viscosity pressure reaches 0.3 P when shock passes Q = 0.043 $\simeq$ 1/2 envelope mass, at age 0.2 yr), which are introduced by the rapid expansion of the vacuum; and (3) by the growing importance of the H_2O opacity as log T drops below 3.4. In Eulerian coordinates, the point $\bar{\tau} = 1$ expands monotonically and its temperature continues to drop. In table 3 we summarize the physical conditions at $\bar{\tau} = 1$ as a function of time.

2. The conditions across the vacuum are characterized by an increasing discontinuity in the physical parameters. The details are summarized in table 4. Until age 0.5 yr, u_b has negative values, reflecting the final envelope pulsation. Then it becomes and remains positive, reaching values well in excess of u_{esc}. The ratio $(\ddot{r}/g)_b$ also becomes large. On the other hand, u_a and $(\ddot{r}/g)_a$ remain negligible. The He-shell remains bound and becomes the surface of a hot star with R $\simeq$ 1.5 $R_\odot$ (see 4. below).

3. The optical depth at point <u>b</u> is initially large (tables 3, 4). It drops and reaches a minimum of $\bar{\tau}_b = 1.9$ at 0.7 yr. Then it rises again as the temperature of the envelope falls below 2500 °K and the H_2O opacity begins to dominate, first in the outer layers and then throughout the envelope. At 2.0 yr, $\bar{\tau}_b$ reaches a maximum and begins to decrease again because of the drop in density. Beyond approximately 5 yr the entire envelope is thin in the continuum.

4. At age zero, the opacity is 0.19 $cm^2\ g^{-1}$ in the He shell and about 1.0 to 20.0 $cm^2\ g^{-1}$ in the lower half of the H-rich envelope. This discontinuity in the opacity is responsible for the initial acceleration of the H-rich envelope and the retention of the He shell. Transfer of momentum and energy from radiation to gas is more efficient in the H-rich material than in He.

Beyond age 0.7 yr, the opacity throughout the H-rich envelope is lower than in the He shell; still the differential acceleration continues. The reason is this. The H-rich envelope has become a highly expanded shell whose inner radius now exceeds $2 \cdot 10^{13}$ cm. The space between this shell and the central star is filled with radiation, most of which originates from the inner surface of the envelope (see equations 4a, c as $X_b \longrightarrow 1$). It is this trapped radiation which pushes on the H-rich envelope.

It is interesting to estimate the acceleration due to this push by applying equation 2 of Paper I to the lower, optically thick part of the H-rich envelope:

$$\frac{\ddot{r}}{g} = -\frac{4\pi r^4}{GM}\frac{\Delta P}{\Delta m} - 1. \qquad (11)$$

For instance, from the data given in table 5 we find that at age 2.7 yr the average value of $\ddot{r}/g$ between Q = 0.0921 and 0.0388 is 1.4.

5. The velocity and mass flow rate, $\dot{m} = 4\pi r^2 \rho u$, are illustrated in figures 1 and 2 as functions of Q and t. The mass flow rate is especially sensitive to the physical and numerical fluctuations discussed under heading 1 above. At age 3 yr, the curve $\dot{m}$ vs. Q has reached a smooth profile. The negative slope implies the formation of a shell (rather than immediate dispersion), since $\partial \dot{m}/\partial m = -\rho^{-1}(\partial \rho / \partial t)\big|_r$. Beyond age 2.5 yr, the entire shell travels at nearly constant velocity. At ages 2.7 and 3.9 yr the velocity equals escape (u = 16 km s^{-1}) and twice escape velocity (u = 24 km s^{-1}) respec-

tively. The physical conditions of the H-rich envelope at 2.7 yr are summarized in table 5.

6. Although convection is generally present in the H-rich envelope out to beyond $\tau = 1$, it carries very little energy. The reason is twofold. The low density ($\rho \lesssim 10^{-9}$ g cm^{-3}) makes convective energy transport very inefficient, while the low value of the opacity ($\kappa \lesssim 5 \cdot 10^{-3}$ cm^2 g^{-1}) enhances the radiative energy transport. The ratio L_{cv}/L remains always less than 0.01. The ratios u_{cv}/u_{sd} and P_{cv}/P become of the order of 0.1 beyond age 2.7. We did not include the pressure due to convection in our computations.

7. To determine the sources and sinks of energy during the ejection, we integrate the equation of conservation of energy (Paper I, equation 15) over the H-rich envelope:

$$\int_{\Delta M_{env}} \left[\frac{\partial}{\partial t}\left(\frac{u^2}{2} - \frac{Gm}{r} + E_{therm} + E_{ex,ion,mol}\right) + \frac{\partial L}{\partial m} + \frac{\partial}{\partial m}\left(4\pi r^2 u P\right)\right] dm = 0, \quad \text{erg s}^{-1}. \tag{12}$$

The terms in this equation express the rate at which kinetic, gravitational, etc. energies are transferred among each other. These rates are summarized for several ages in table 6. In general, the gravitational, kinetic, and photon terms are energy sinks, while the other terms are energy sources. The dominant energy source is the mechanical term: radiation trapped in the vacuum is pushing on the envelope. Until about age 3.5 yr, electron recombination and molecule formation contribute more energy than thermal cooling. Initially the greatest energy sink is gravitation, while after 2.3 yr. most of the available energy goes into the kinetic term. The photon term is always less than the other sinks of energy.

In figure 3 we illustrate the gravitational, kinetic, and total energies

of the H-rich envelope as functions of time. The zero point of the contribution of excitation, ionization, and molecular binding energies are set at atomic neutrality. The entries in table 6 are the slopes of the curves of figure 3.

Finally, we shall compute the numerical accuracy and self-consistency of our results by checking the conservation of energy in the H-rich envelope. In the last column of table 6 we list the per cent error in the time rates of energy,

$$\frac{100\ \left|\sum \dot{E}\right|}{\sum \left|\dot{E}\right|}\ , \tag{13}$$

where the summation includes all terms of equation 12. This error is about 0.1 % or less except near age 0, where it is of the order of 5 %.

c. Expansion of the H-rich envelope, without H_2O opacity

In table 7 we summarize the results of the run without H_2O opacity at age 0.62 yr. The base of the envelope is still optically thick, and the velocity is roughly 1/3 to 1/2 of escape velocity. The high luminosity inside the envelope is due to mechanical compression. Up to this age the results are qualitatively like those of the run with H_2O opacity. However only 0.1 yr later, the H-rich envelope becomes optically thin because of the rapid decline of the opacity to the order of 10^{-5} cm^2 g^{-1}. Escape velocity has not yet been reached.

At this point we had to terminate the computations because the diffusion approximation becomes invalid. We suspect that ejection might still occur, especially if line opacities were included. A hydrodynamic atmosphere code is required to test this hypothesis. At any rate, we feel that the ejection results that include H_2O opacity are the more realistic ones and in the next section we shall base our conclusions on those.

V. Discussion

We have found that the H-rich envelope of an evolved red giant near 1 $M_\odot$ is ejected as the luminosity approaches 19000 $L_\odot$. We associate this ejection with the formation of planetary nebulae. The core and envelope masses and the luminosity of our stellar model lie in the ranges observed for planetary nuclei and nebulae. The stellar remnant has an effective temperature of a few 10^5 °K and a radius of about 1.5 $R_\odot$. It evolves within a few 10^4 yr to a hot blue star and some 10^5 yr later to a white dwarf (Kutter 1971). These stellar evolution results agree with the observations of planetary nuclei (Abell and Goldreich 1966, Osterbrock 1966, O'Dell 1968).

Our ejection results contain a number of interesting features, most of which are confirmed by observations. The others are predictions (points 1 and 2 below), whose tests depend on observing the actual formation of a planetary nebula.

(1) LPV pulsation seems to always preceed ejection. This result is confirmed by Wood's (1973) theoretical investigation.

(2) Ejection occurs on a time scale of a few LPV pulsation periods.

(3) The entire H-rich envelope is ejected. This corresponds to the "clean separation" suggested by Osterbrock (1966). We suspect, however, that in reality traces of H-rich material remain on the central star, because (1) our vacuum, which is void of any matter, is merely an idealization of the actual case and (2) during the star's earlier evolution some mixing of H-rich material and He may well have occurred. Still, in some cases the star may appear to be H-poor. The subsequent contraction of these traces of H-rich material onto the stellar surface might be responsible for the temporary rise in the luminosity observed in nuclei of young planetary nebulae (Deinzer and Hansen 1969). This luminosity rise would occur on a time scale equal

to the diffusion time scale of radiation through the contracting material.

(4) The H-rich envelope is ejected as a shell.

(5) It attains velocities in the range of 20 to 30 km s^{-1}. Ionization, excitation, and molecular binding energies contribute noticeably to the final kinetic energy. For instance, in Paper II these energies were neglected and the final velocities were only about 2 km s^{-1}.

(6) The low temperature of about 1000 °K which our envelope reaches would be a prerequisite for grain formation. Molecules and grains have been observed in planetary nebulae (Ulrich et al. 1966; Gillett, Low, and Stein 1967; Zappala 1967). Only after the entire envelope becomes optically thin, can the ultraviolet radiation from the central star heat the nebula to the observed temperatures of about 10^4 °K.

(7) The ejection mechanism depends on the existence of a H-rich envelope surrounding a stellar core and a sufficiently high luminosity. Since interior studies indicate that such luminosities are attained or exceeded by virtually all red giants near or above one solar mass as the He shell-burning advances toward the surface, this ejection mechanism is a common one. Such a common mechanism is required to explain the high frequency of planetary nebula formation, $\simeq$ 1 p.n./yr/Galaxy, which corresponds approximately to the birth rate of stars in the same mass range (Abell and Goldreich 1966, Weidemann 1967). There may exist an upper mass limit on the precursor stars; but as long as it is above 1.5 or 2.0 $M_\odot$ it would not greatly affect the statistics.

(8) We have assumed that a vacuum is created between escaping envelope and stellar remnant. The same assumption was made by Milne (1930) in his study of the effect of radiation from a central point source on a planetary nebula. In reality the space between star and nebula probably contains some matter, but with a density $\ll$ nebula density. Most likely, convection would

be either absent (because P_g/P is low, Kutter 1970) or inefficient in this space. Hence, energy will be transported mainly by radiation and thus provide the "radiative piston" required for a shell ejection. These results are in discord with the view of Joss et al. (1973) who suggest that energy transport by convection will make radiation ineffective in ejecting the envelope.

In conclusion, we feel that these results and those published earlier by us and others provide a satisfactory explanation of the basic mechanism of the ejection of planetary nebulae and the evolution of the central stars. However, many details still need to be answered. In particular, the later stages of ejection should be studied using the radiative transfer equation. The stellar core and envelope masses should be varied to determine the range over which this ejection mechanism applies. Finally, non-spherical effects such as rotation, magnetic fields, presence of stellar companions, and interaction with the interstellar medium should be investigated.

REFERENCES

Abell, G. O., and Goldreich, P. 1966, Pub. A.S.P., 78, 232.

Allen, C. W. 1963, Astrophysical Quantities, 2nd Ed. (New York: Oxford University Press).

Aller, L. H. 1961, The Abundance of the Elements (New York: Interscience Publishers).

Auman, J. R. 1966, Ap. J. Suppl., 14, 171.

Auman, J. R., and Bodenheimer, P. 1967, Ap. J., 149, 641.

Deinzer, W., and Hansen, C. J. 1969, Astr. and Ap., 3, 214.

Gillett, F. C., Low, F. J., and Stein, W. A. 1967, Ap. J. (Letters), 149, L97.

Jeans, J. H. 1923, M.N.R.A.S., 83, 481.

Joss, P. C., Salpeter, E. E., and Ostriker, J. P. 1973, Ap. J., 181, 429.

Keeley, D. A. 1970, Ap. J., 161, 657.

Kutter, G. S. 1970, Ap. J., 160, 369.

_____. 1971, ibid., 164, 115.

Kutter, G. S., Savedoff, M. P., and Schuerman, D. W. 1969, Ap. and Space Sci., 3, 182.

Kutter, G. S., and Sparks, W. M. 1972, Ap. J., 175, 407 (Paper I).

Milne, E. A. 1930, Z.f. Ap., 1, 98.

O'Dell, C. R. 1968, in I.A.U. Symp. No. 34, ed. D. E. Osterbrock and C. R. O'Dell (Dordrecht: D. Reidel Publishing Co.) pp. 361-375.

Osterbrock, D. E. 1966, in Stellar Evolution, ed. R. F. Stein and A. G. Cameron (New York: Plenum Press), pp. 381-387.

Paczyński, B., and Ziołkowski, J. 1968a, Acta Asir., 18, 255.

_____. 1968b, in I.A.U. Symp. No. 34, ed. D. E. Osterbrock and C. R. O'Dell (Dordrecht: D. Reidel Publishing Co.), pp. 396-399.

Rose, W. K., and Smith, R. L. 1970, Ap. J., 159, 903.

Sparks, W. M. and Kutter, G. S. 1971, BAAS, 3, 484.

_____. 1972, Ap. J., 175, 707 (Paper II).

_____. 1973, Memoires Societe Royale des Science de Liege, 6th series, 5, 457.

Talbot, R. J. 1971a, Ap. J., 163, 17.

_____. 1971b, Ap. J., 165, 121.

Weideman, V. 1968, in I.A.U. Symposium No. 34, ed. D. E. Osterbrock and C. R. O'Dell (Dordrecht: D. Reidel Publishing Co.), pp. 423-424.

Ulrich, B. T., Neugebauer, G., McCammon, D., Leighton, R. B., Hughes, E. E., and Becklin, E. 1966, Ap. J., 146, 288.

Wood, P. R. 1973, preprint.

Zappala, R. R. 1967, Ap. J. (Letters), 148, L81.

$L/L_\odot$	log r	log T	period (yr)
3100	13.04	3.55	0.5
6500	13.25	3.54	1.1
9200	13.31	3.53	1.4
12000	13.36	3.53	1.7

Table 1. Time-averaged conditions at optical depth 1 during the long-period variable phase of the H-rich envelope.

$Q = 1 - \frac{m}{M}$	log r	log T	log P	log ρ	κ ($cm^2 g^{-1}$)	τ
0.0921	11.005	5.585	7.754	-9.203	0.78	1.1 (5)
0.0681	13.366	4.248	3.490	-8.830	4.82	9.1 (4)
0.0464	13.421	3.966	3.267	-8.565	6.75	5.4 (3)
0.0235	13.443	3.535	2.921	-8.364	4.9 (-4)	1.0
0.0119	13.454	3.457	2.592	-8.553	1.5 (-4)	0.26

Table 2. Physical conditions of H-rich envelope at age zero. L = 19000 $L_\odot$. The envelope is convective to τ = 0.19 (Q = 0.0096).

age (yr)	Q	log r	u (cm s^{-1})	u/u_{esc}	log T	log P	log ρ	L/L_{θ}	L_{cv}/L
1.00	.0174	13.779	1.04 (6)	0.47	3.335	0.923	-10.112	19222	1.1 (-7)
2.00	.0255	13.947	1.04 (6)	0.58	3.241	0.719	-10.112	19778	4.9 (-4)
3.00	.0360	14.122	1.77 (6)	1.22	3.164	0.978	-9.702	19547	1.0 (-2)

Table 3. Physical conditions at optical depth 1 of H-rich envelope as function of time.

age (yr)	log r_b	u_b (cm s^{-1})	$(u/u_{sound})_b$	$(u/u_{esc})_b$	$(\ddot{r}/g)_b$	log T_b	log P_b	log $\rho_{18+1/2}$	$\kappa_{18+1/2}$ (cm^2 g^{-1})	τ_b
0.51	13.167	2.25 (5)	3.0 (-2)	5.3 (-2)	0.66	4.510	3.686	-9.205	0.97	9.2 (3)
1.00	13.689	1.11 (6)	0.28	0.48	-0.57	3.429	2.274	-8.844	9.2 (-5)	2.2
2.00	13.916	1.31 (6)	0.34	0.73	1.2	3.376	1.821	-9.246	6.8 (-4)	3.1
3.00	14.115	1.78 (6)	0.46	1.3	3.4	3.242	1.421	-9.405	1.7 (-3)	2.1
3.99	14.298	2.52 (6)	1.2	2.2	7.7	3.119	1.055	-9.586	2.7 (-3)	1.5

Table 4. Vacuum conditions. The following parameters remain approximately constant: log r_a = 11.005, $u_a \simeq -0.1$ cm s^{-1}, $(\ddot{r}/g)_a \simeq 10^{-10}$, log T_a = 5.591, log P_a = 7.465, log $\rho_{18-1/2}$ = -2.678, $L_a = L_b$ = 19000 $L_\odot$.

age (yr)	$\dot{E}_{grav}/L_\odot$	$\dot{E}_{kin}/L_\odot$	$\dot{E}_{phot}/L_\odot$	$\dot{E}_{mech}/L_\odot$	$\dot{E}_{therm}/L_\odot$	$\dot{E}_{ex,ion,mol}/L_\odot$	% error
1.00	2516.	-857.	457.	-1528.	-90.	-503.	0.1
2.00	1057.	721.	872.	-1796.	-99	-756.	0.02
2.68	774.	1448.	750.	-2274.	-68.	-632.	0.03
3.00	673.	1824.	519.	-2474.	-53.	-491.	0.03
3.86	455.	2918.	39.	-3392.	-23.	1.	0.03

Table 6. Time rate of change of gravitational, kinetic, photon, mechanical, thermal, and sum of excitation, ionization, and molecular energies of H-rich envelope as function of time. At age 2.68 yr, the envelope reaches escape velocity. The last column is the quantity $100 \cdot \left| \sum \dot{E} \right| / \sum \left| \dot{E} \right|$.

Q	log r	u/u_{sound}	$\ddot{r}/g$	$\dot{m}(M_\odot yr^{-1})$	log T	log P	log ρ	L_{cv}/L	κ (cm^2g^{-1})	τ
0.0921	14.0552	1.8	1.1	1.8	3.283	1.541	-9.357	0.0	1.4 (-3)	2.32
0.0658	14.0585	1.8	1.0	1.6	3.255	1.434	-9.409	8.2 (-3)	1.6 (-3)	1.81
0.0388	14.0623	1.7	1.9	1.3	3.210	1.245	-9.512	7.5 (-3)	1.9 (-3)	1.21
0.0126	14.0678	6.0	2.4	0.7	3.097	0.823	-9.790	5.5 (-6)	3.0 (-3)	0.5

Table 5. Physical conditions of H-rich envelope at age 2.68 yr. The following parameters are nearly constant: u = 16 km s^{-1}, u/u_{esc} = 1.0, L = 19000 $L_\odot$, pressure scale height = $6.0 \cdot 10^{12}$ cm. The photon diffusion time scale between Q = 0.0921 and 0.0126 is of the order of 0.01 yr.

Q	log r	u (cm s^{-1})	u/u_{sound}	u/u_{esc}	$m(M_\odot yr^{-1})$	log T	log P	log ρ	$L/L_\odot$	L/L_{cv}	$\kappa(cm^2 g^{-1})$	τ
0.0921	13.244	1.21 (6)	0.17	0.31	4.3 (-2)	4.438	3.459	-9.309	19005	0.0	0.93	2.7 (3)
0.0891	13.312	1.23 (6)	0.49	0.34	4.4 (-2)	4.296	3.080	-9.434	23059	0.34	1.27	1.4 (3)
0.0834	13.417	1.72 (6)	1.5	0.54	6.2 (-2)	3.636	1.792	-9.608	85793	0.13	4.0 (-4)	1.4
0.0780	13.493	1.57 (6)	2.6	0.53	5.9 (-2)	3.588	1.604	-9.748	83013	0.0	2.3 (-4)	1.0
0.0729	13.554	1.75 (6)	3.0	0.64	7.3 (-2)	3.565	1.558	-9.771	81244	0.0	1.9 (-4)	0.85

Table 7. Physical conditions of H-rich envelope, not including H_2O opacities, at age 0.62 yr.

log r_a = 11.005, u_a = -0.199 cm s^{-1}, log T_a = 5.591, log P_a = 7.465, log $\rho_{18-1/2}$ = -2.678, L_a = 19000 $L_\odot$.

Captions of Figures

Figure 1. - Velocity as function of Q and time.

Figure 2. - Eulerian rate of mass flow as function of Q and time. Points at optical depth 1 are indicated by vertical line.

Figure 3. - Gravitational, internal, kinetic, and total ($E_{grav} + E_{int} + E_{kin}$) energies of H-rich envelope vs. time. Internal energy is sum of thermal, excitation, ionization, and molecular contributions, with zero point set at atomic neutrality. Solid curves are positive, dashed curves are negative. Points at optical depth 1 are indicated by vertical line.

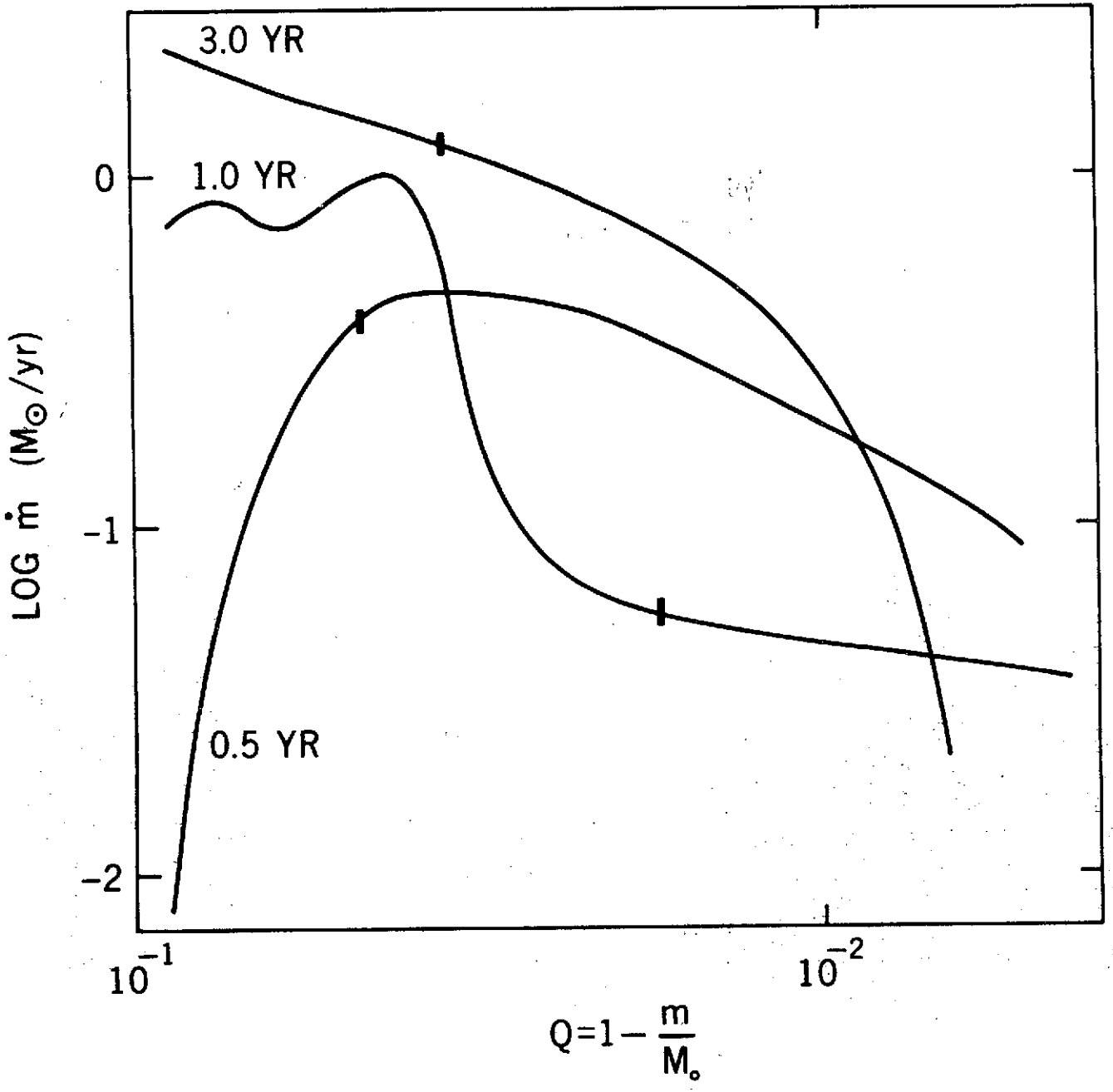
3.0 YR
1.0 YR
0.5 YR
0
-1
-2
LOG ṁ (M⊙/yr)
10^-1
10^-2
Q=1−m/M⊙

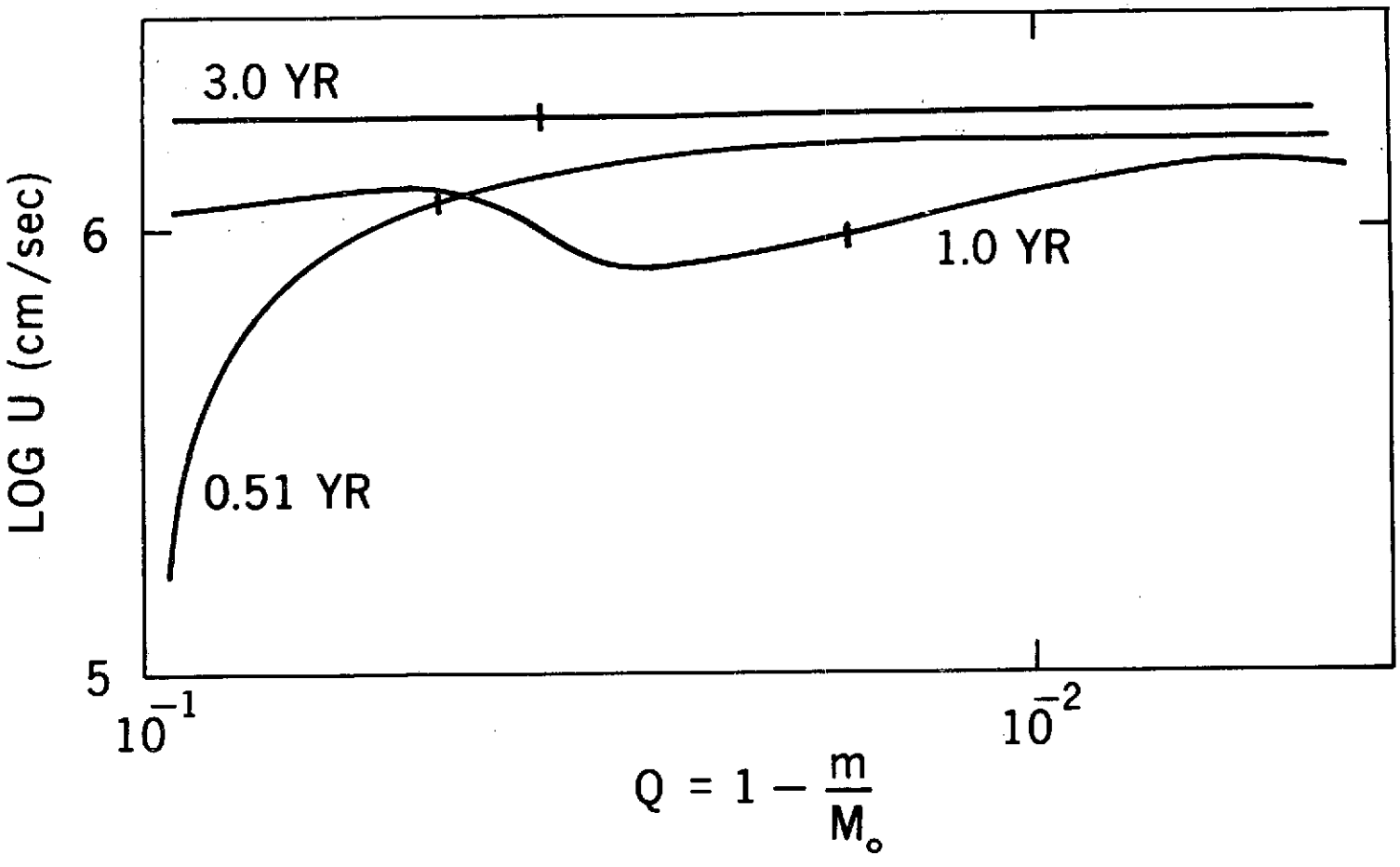
3.0 YR
1.0 YR
0.51 YR
LOG U (cm/sec)
6
5
10^{-1}
10^{-2}
$Q = 1 - \frac{m}{M_\circ}$

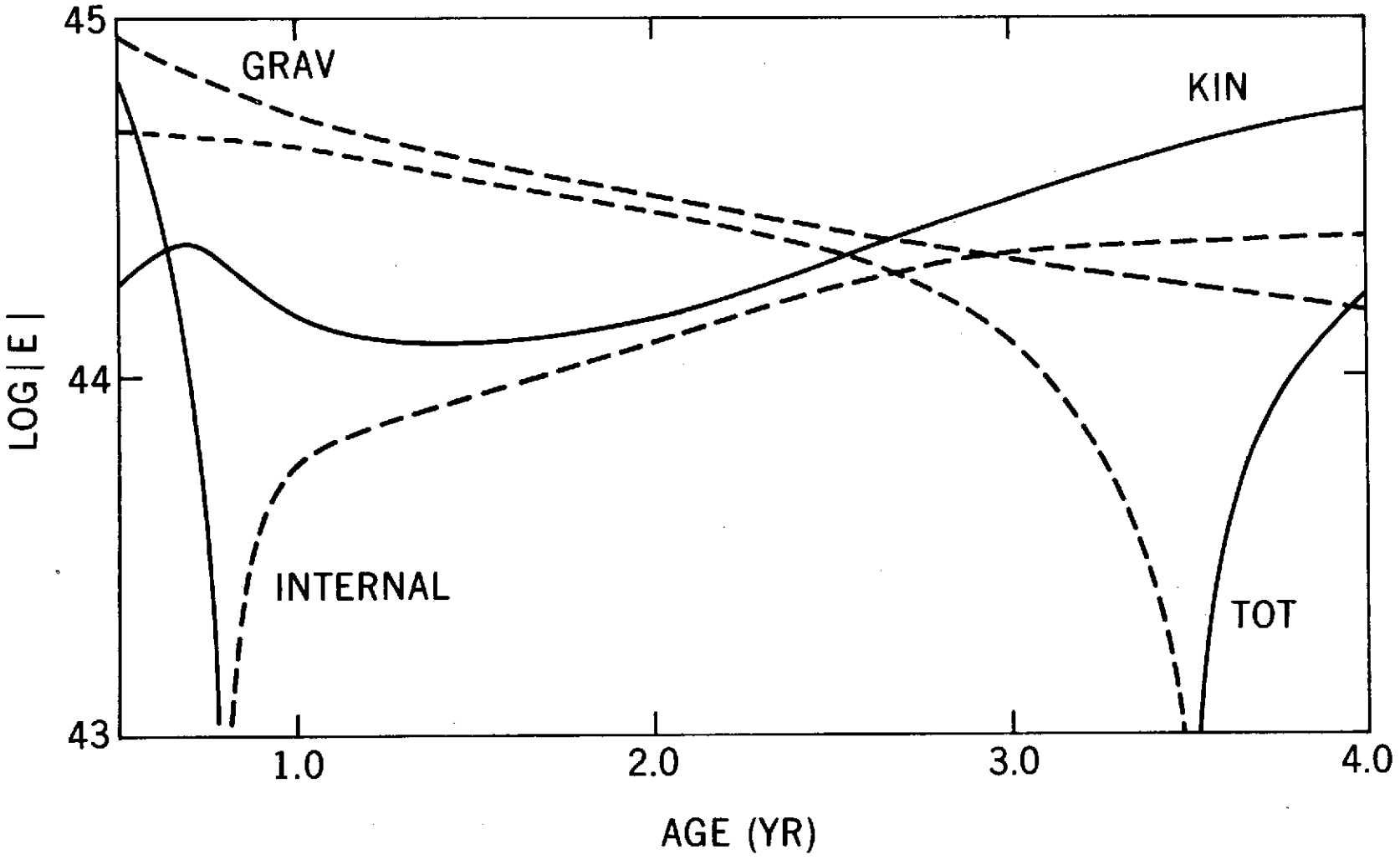

NASA–GSFC